An Experimental Study of the Boundary Layers on Low-Temperature Subliming Ablators

FRED LIPFERT* AND JOHN GENOVESE†
General Applied Science Laboratories, Inc., Westbury, N. Y.

An experimental program was carried out to develop model fabrication techniques and instrumentation necessary to provide fundamental data on ablating boundary layers. Subliming ablators were chosen to simplify the physical and chemical properties at the wall. Two low-temperature materials, dry ice and camphor, were selected in order to simulate re-entry ablation under the limitations imposed by the test facility. Instrumentation developed in the program included direct surface recession measurements during the test, gas sampling probes, and a boundary-layer survey apparatus. The test program included a non-ablating steel cone instrumented for surface pressure and heat-transfer measurements. Ablating models were steel-tipped 15° half-angle cones tested at Mach 6 with unit Reynolds numbers from 3 to 4 × 10^5/in. Results indicate that meaningful measurements of boundary-layer parameters can successfully be obtained from the surface of low-temperature subliming ablators.

Nomenclature

C_β = blowing coefficient
C_f = skin-friction coefficient
C_{f0} = nonblowing skin-friction coefficient
C_p = constant pressure specific heat
h = static enthalpy
H = stagnation enthalpy
H_{eff} = effective heat of ablation
k = a constant depending upon the state of the boundary layer, i.e., laminar or turbulent
$\mathfrak{L}$ = heat of sublimation
m = molecular weight
$\dot{m}$ = mass flow
Pr = Prandtl number
$\dot{q}$ = aerodynamic heat transfer
Re = Reynolds number
T = temperature
u = velocity
y = vertical coordinate
γ = ratio of specific heats
δ = boundary-layer thickness
ζ = blowing parameter
ρ = density

Subscripts

1 = sublimed specie
2 = external flow specie
w = wall conditions
0 = stagnation conditions; value with no blowing
in = initial conditions
b = body conditions
e = inviscid edge conditions
r = recovery conditions
subl = sublimation
eff = effective
∞ = freestream
mix = test facility mixing chamber conditions

Presented as Paper 69-152 at the AIAA 7th Aerospace Sciences Meeting, New York, January 20–22, 1969; submitted January 27, 1969; revision received September 23, 1970. The bulk of this work was supported by the Advanced Research Projects Agency under Contract DA-49-083 OSA-3135, ARPA Order No. 396.

* Manager, Flight Sciences Section. Member AIAA.
† Senior Scientist, Thermochemistry and Viscous Flow Section; presently with American Standard, Research Division. Member AIAA.

Introduction

ABLATION has long been recognized as an effective thermal protection system for re-entry vehicles, the design of which had historically been based on global concepts such as the "effective heat of ablation".[1] However, subsequent consideration of the ablation effects on vehicle dynamics placed emphasis on local ablation phenomena[2,3] that might result in asymmetries, particularly for slender body shapes.

This paper discusses a program that was intended to provide fundamental data on ablating boundary layers by developing the technology required to make local, detailed measurements under turbulent, ablating conditions. Such data had not appeared in the literature at the time this program was conceived, although much had been accomplished with transpiration of various gases through porous model walls. Since ablating surfaces provide exact coupling between heat transfer and mass injection rates, including effects on boundary-layer transition, such tests were to be preferred for re-entry body technology, particularly from the standpoint of studying asymmetric local surface phenomena.

Subliming materials were selected because of the simplified chemical and physical properties at the wall. Low-temperature materials were to be used because of the desire to simulate re-entry blowing rates using a conventional wind tunnel. The emphasis was on development of experimental techniques that would allow direct measurement of boundary-layer properties. A more complete account of the project is given in Ref. 4.

Simulation Criteria

The aerodynamic influence of ablation acts through its alteration of body geometry and its effect on boundary-layer separation, transition, and displacement thickness. This mechanism involves the interaction of the inviscid flow, boundary layer, and the subliming ablator and, if properly simulated, insures correct scaling of changes in body geometry. A general discussion of ablation testing and simulation is given in Ref. 5, and Libby[6] has analyzed the similarity requirements for subliming bodies in some detail, under the assumptions of unsteady sublimation and laminar flow. Rigorous treatment of the turbulent case requires consideration of the turbulent transport properties. However,

physical reasoning indicates that satisfaction of the similarity requirements for laminar flow through duplication of the Reynolds number, pressure and injection velocity distributions, and molecular properties will allow simulation of the transition location and the downstream turbulent boundary layer.

The effects of nose blunting are excluded in the present study. The assumption of steady flow and high Mach numbers with the added constraint of zero angle of attack eliminates the necessity of duplicating the external flow Mach number except for possible effects on transition and interactions near the nose. Possible interaction effects in the nose region will not be simulated; they are also of no interest here.

Since only sharp-nosed conical bodies are under consideration, the pressure distribution automatically duplicates that on the re-entry vehicle. The heat-transfer distribution is also matched, provided that the wall-temperature ratio is duplicated; thus the injection velocity distribution is preserved.

To summarize, by restricting the program to sharp-nosed cones at zero angle of attack and steady ablation in air, Libby's set of simulation requirements can be reduced to the following:

a) m_2/m_1 ; b) C_{P_1}/C_{P_2} ;

c) Re; d) $\mathfrak{L}/h_{0,e}$;

e) $C_{P_b}T_{in}/h_{0,e}$; f) $\mathfrak{L}/[C_{P_b}(T_{subl}-T_{in})_b]$

Past considerations of the necessary similarity requirements for subliming bodies[7] have produced two parameters: the blowing coefficient C_β and the blowing parameter ζ as defined by

$$\zeta \equiv 2C_\beta/C_f \tag{1}$$

where $C_\beta \equiv \rho_w\mu_w/\rho_e u_e$. The analysis of Ref. 7 indicates that ζ is the parameter of prime interest. If we express the blowing parameter in terms of the turbulent boundary-layer heat transfer and the effective heat of ablation,[1] all of the simulation parameters derived in Libby's analysis are utilized with the exception of C_{P_1}/C_{P_2}, i.e.,

$$\zeta = \frac{(H_r - H_w)}{Pr^{2/3}\,[H_{eff} - k(H_r - h_w)]} \tag{2}$$

where

$$H_{eff} = \mathfrak{L} + C_{Psolid}(T_w - T_{in}) + k(H_r - h_w) \tag{3}$$

Implicit in the expression for the blowing parameter are the following relations[1] for the aerodynamic heating and skin-friction ratio C_f/C_{f_0}:

$$\dot{q} = [\rho_e u_e(H_r - H_w)C_f]/2Pr^{2/3} \tag{4}$$

$$C_f/C_{f_0} = 1 + k[(H_r - h_w)/H_{eff}] \tag{5}$$

The constant k is a function of the molecular weight ratio m_1/m_2 and the nature of the boundary layer. Thus, ζ depends upon Pr, $\mathfrak{L}/h_{0,e}$ (which is approximately $\mathfrak{L}/H_r$), m_1/m_2, and $h_w/h_{0,e}$. Specification of C_{P_1}/C_{P_2} completes the list.

The two parameters ζ and the ratio of specific heats C_{P_1}/C_{P_2} are used as the governing similarity requirements in the present study.

Material Selection

During an extensive materials evaluation program, about 100 organic and inorganic candidate materials were investigated. The possibilities were narrowed to those materials that were solids with low melting points under standard atmospheric conditions in order to ease model fabrication.

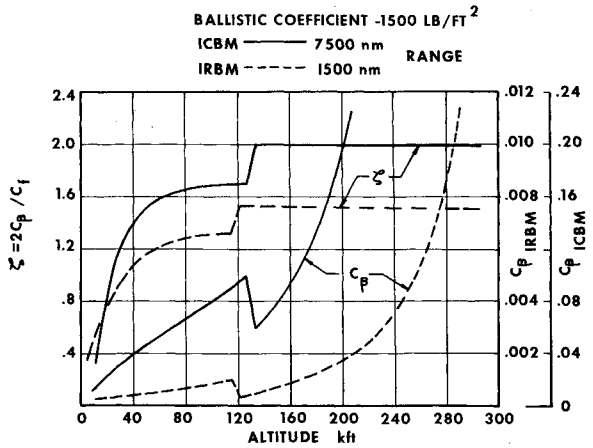

Fig. 1 Variation of blowing parameter and blowing coefficient with altitude.

Compounds that generated chemically simple and nonreactive products of ablation were of particular interest. Those first rejected were eliminated from consideration for two main reasons: either they were dangerous to handle, being extremely toxic or strong local irritants, or they generated highly explosive or poisonous fumes when heated. Since the present study was only concerned with subliming ablation, materials that would melt rather than sublime, within the range of test conditions used in the experiments, were also discarded. Several decomposing compounds were eliminated because of an anticipated lack of structural strength. From the candidate materials that were considered, four were selected for serious consideration: carbon dioxide (dry ice), camphor, napthalene, and paradichlorobenzene. Suitable model fabrication techniques were developed for all four, but testing was limited to dry ice and camphor. This was done because it was not possible to guarantee, a priori, that the test conditions would preclude melting rather than sublimation of napthalene and paradichlorobenzene.

Test Conditions and Flight Simulation

Typical conical body re-entry trajectories were computed using a two-degree-of-freedom trajectory program and empirical relations for Teflon‡ sublimation, considering only perfect gas heat transfer. These established within reasonable accuracy the range of values of blowing coefficient (C_β) and blowing parameter (ζ) to be simulated. The results of the computations for ICBM and IRBM trajectories are presented in Fig. 1 for a point 1 ft from the nose of the body.

Test conditions were selected from the standpoint of matching the simulation requirements as nearly as possible with existing equipment. It was therefore decided to use the GASL Pebble Bed Wind Tunnel Facility, with a free-stream Mach number of 6. This facility has a double throat nozzle system that allows cold air to be added and mixed to overcome the heater mass flow limitation and achieve higher unit Reynolds numbers, albeit at the expense of stagnation enthalpy. The envelope of ablating tunnel test conditions is shown in Fig. 2; the data points represent conditions at which tunnel calibration tests were run.

Table 1 presents the pertinent physical properties and several of the simulation parameters of the four candidate materials, together with Teflon, the flight ablator being simulated. It is seen that dry ice provides the best simulation in terms of specific heats and wall-temperature ratio, and

‡ Dupont registered trademark.

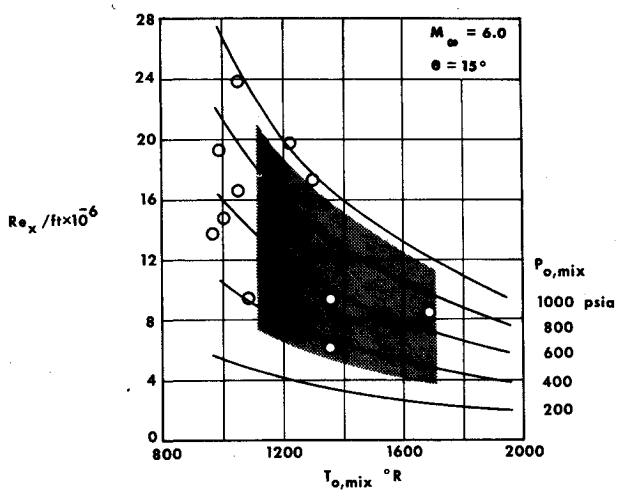

Fig. 2 Range of test conditions.

paradichlorobenzene comes closest in terms of the ratio of sublimation-to-recovery enthalpy. Camphor has the best simulation of sublimation and conducting heat fluxes.

Steel Calibration Model

The "baseline" model was a 15° half-angle cone 12 in. long, fabricated from stainless steel, as shown in Fig. 3. The skin thickness was 0.100 in. from the 3- to 11-in. stations, measured along the cone surface. Pressure taps were installed every $\frac{1}{2}$ in. along the 0° ray and every inch along the 180° ray. Surface thermocouples were installed every $\frac{1}{2}$ in. along both 90° and 270° rays. A detailed description of the thermocouple and pressure tap installation is given in Ref. 4.

Prior to the test programs, the model had a highly polished finish (but not mirror) that deteriorated during testing because of the "sand-blasting" effect of particles in the wind-tunnel flow from the heater. The finish at the end of the test program was estimated at #63 ground finish. The nose radius was 0.020 in.

Later in the test program, the steel model was adapted for cold-wall heat-transfer tests by spraying liquid nitrogen into the interior cavity prior to testing.

Dry-Ice Models

Except for its low temperature (−109°F), which necessitates the use of heavily insulated gloves during handling, dry ice is an ideal raw material for model fabrication. It is easily sawed, drilled, or tapped and can be machined to a good finish. However, its high sublimation rate at atmospheric conditions complicates machining operations because of the difficulty of mounting and holding a block; lathe operation proved to be impractical for this reason.

A new approach based on a technique suggested in Ref. 8 was tried and found to give satisfactory results. A rotating

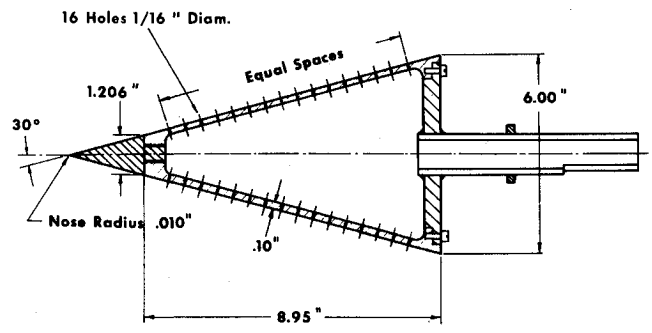

Fig. 3 Steel calibration cone.

Table 1 Comparison of final material properties

	Teflon	CO_2	Camphor	Naphthalene	Paradichlorobenzene
Molecular weight	100	44	152	128	147
Formula	C_2F_4	Co_2	$C_{10}H_{16}O$	$C_{10}H_8$	$C_6H_4Cl_2$
$\mathcal{L}(H_{subl})$, Btu/lb	750	240	151	237	140
ρ_{solid}, lb/ft³	137	100	62	71.5	48
T_{subl}, °R	1800	300	720	636	648
C_P solid, Btu/lb-°R	0.3	0.303	0.387	0.281	0.219
$\lambda_{solid} \times 10^{-5}$ Btu/ft/sec/°F	4	7.2	3.2	6	—
$H_{eff\ lam}$,[a] Btu/lb	3100	546	376	465	252
$H_{eff\ turb}$,[a] Btu/lb	1500	351	292	377	177
$C_{P\ gas}$ at T_{subl}	0.288	0.170	~0.46[b]	~0.4[b]	~0.3
$C_{P\ gas}$ at $T_{a,w}$	0.317	0.286	~0.6	~0.5[b]	~0.4
H_r, Btu/lb	4560	400	400	400	400
R_e[a]	10^7–10^8	10^6–10^7	10^6–10^7	10^6–10^7	10^6–10^7
Mach number (M_∞)[a]	10–20	6	6	6	6
h_w/H_r	0.1	0.18	0.43	0.38	0.39
$\mathcal{L}/H_r$	0.165	0.6	0.38	0.59	0.35
$(H_{eff}/H_r)_{turb}$	0.328	0.88	0.73	0.94	0.44
$\mathcal{L}/[C_{Pb}(T_{subl} - T_m)_b]$	2	—	2	8	5.4

[a] Typical conditions.
[b] Estimated from data for similar compounds.

shaping tool was fabricated consisting of two cutting edges set at the desired cone semivertex angle from the axis of rotation, with a length somewhat greater than the desired slant height of the cone. This tool was mounted in a drill press and forced into the ice block, cutting away the outside of the block and leaving a cone-cylinder, which was then trimmed to the final shape. The models were made one at a time just prior to testing and were quickly mounted in the wind tunnel and held in place with liquid-nitrogen-cooled hardware, as shown in Fig. 4.

The fit between the beginning of the ice cone frustrum and the steel nose varied somewhat from model to model and is recorded in the results as either a forward- or rearward-facing step.

After several unsuccessful attempts at instrumenting these models in the time available, it was decided that only non-instrumented dry-ice cones would be tested.

Camphor Models

The minimum tunnel static pressure level precluded the use of both paradichlorobenzene and naphthalene. This left camphor for the second model material. Since cone surface data were of interest (with the decision to fabricate noninstrumented dry-ice models), particular emphasis was placed on producing instrumented camphor models. A casting technique that permitted the installation of sensors within the ablative material was developed. The models were successfully formed by casting a thick layer of camphor around a steel-tipped aluminum mandrel. Details of the apparatus and techniques employed in the operation are contained in Ref. 4.

In every case, a newly cast model emerged from the mold with a white frosting approximately $\frac{1}{16}$ in. thick. The models were subsequently machined to give flush fitting noses, and this layer was removed.

The first three models spalled very badly as the tunnel was shut down at the termination of the test. The camphor layer appeared to be ripped off first at the base and then further forward. Since preservation of the surface detail formed during the testing was a program objective, a back plate was screwed to the mandrel base to shield the camphor. This relieved the spalling to some degree, although it was never completely eliminated.

Instrumentation

In addition to conventional boundary-layer survey apparatus, pressure probes, and thermocouples, several new

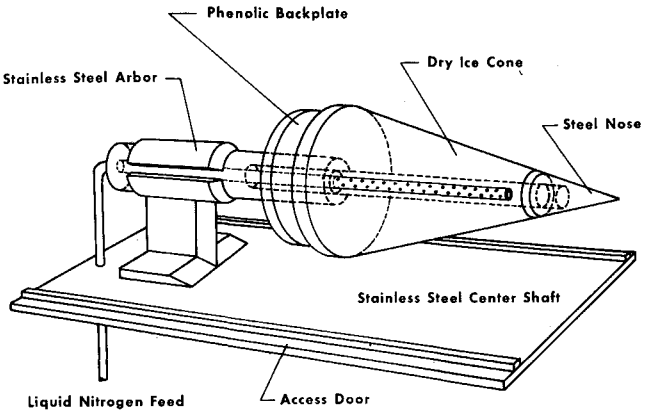

Fig. 4 Dry ice model installation and hardware.

types of equipment were designed and built. The need for recession-rate data and boundary-layer profiles on receding surfaces led to the development of a laser-powered surface follower. Ultimately this device could be used to control the position of an array of boundary-layer probes in relation to ablating surfaces. The use of aromatic hydrocarbon ablatives required gas-sampling probes that would prevent any chemical alteration of the sample after it entered the probe. This led to the development of "quenching" probes that bled cold helium into the stagnation chamber within the probe. A brief discussion of these devices, along with the other instrumentation used in the program, is contained in the following sections.

Photographic Equipment

All tests with ablating models were filmed by a high-speed motion-picture camera. The film provided detailed histories of the formation of wedge-shaped recesses on the cone surface. The presence of waffle patterns on the surface of both camphor and dry-ice cones was noted during post-test examinations, but, because of a lack of sufficient contrast, these phenomena do not appear on the film. In addition, a 35-mm "robot" camera was used to photograph the model at predetermined intervals ranging from 1 to 2 sec during the test. Enlargements of these photographs provided the body geometry history used to compute recession-rate data.

Laser Surface Follower

A special laser-powered device was designed and built to measure the recession rate of ablating bodies without causing flowfield interference that might alter the local ablation rate. The principle of operation is basically conversion of the translating motion of the laser spot on the cone surface to an angular deflection, which is then sensed by a photocell detector and read-out through a servo loop. Referring to Fig. 5, as the surface recedes, the photocell detector "sees" the laser spot at a different location on the image-bending mirror, which is set at an angle that magnifies the movement of the original light spot on the cone. Any movement seen by the photocell detector results in an electrical imbalance, which is used to signal the servo motor to translate the displacement lens in such a way as to compensate for the movement and to restore the balance. The movement of this displacement lens is thus proportional to the cone surface recession and is recorded on an oscillograph. Thickness gages were used for calibration of the device in situ.

One difficulty that was encountered with some of the materials on which measurements were taken was that the surface was or became somewhat translucent during the test. In this case, the location of the effective optical reflecting "surface" is different from that of the true surface, and, additionally, the image becomes distorted and weak at the

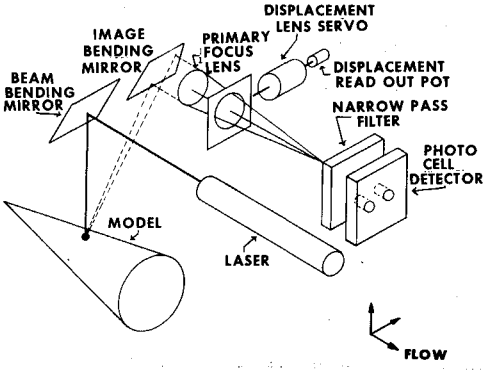

Fig. 5 Laser surface follower schematic.

detector cell. These combined effects, at the most, could produce an uncertainty on the order of 0.005 in.

Camphor Model Instrumentation

Three types of information were desired from the instrumentation mounted on the camphor models: the cone surface static pressure, the model surface temperature, and some data on the recession rate of the ablating surface. The recession-rate data were needed as a check on the surface recession histories obtained from both the laser device described previously and the enlarged photographs.

The cone surface static pressure was measured by a surface pressure tap made by drilling a 0.067-in.-diam hole through the aluminum mandrel. The tube end of a $\frac{1}{16}$-in. diameter to $\frac{1}{4}$-in. tubing reducer was epoxied into the hole from the inside. After the ablative liner had been cast around the mandrel, the pressure tap hole was drilled through to the surface of the camphor from the inside.

The cone surface temperature was measured by chromel-alumel thermocouples mounted in $\frac{1}{16}$-in.-diam stainless tubing that had been secured to the mandrel in various locations at specified heights. The camphor ablator was then cast over the tubes, embedding them in the material. During the test, the surface temperature was recorded at the instant the receding surface exposed the thermocouple head. This device was employed on only two tests. In the first, the thermocouples were not exposed, and no temperature changes were recorded. In the second test, one thermocouple was exposed and attained the temperature level expected for the ablating camphor.

As a check on surface recession rates, buried stagnation pressure probes were used to indicate the position of the ablating surface by their exposure and subsequent change in pressure level. Proper positioning and tip orientation were assured by soldering the probes to a steel collar that could be attached to the cone mandrel by two screws prior to casting.

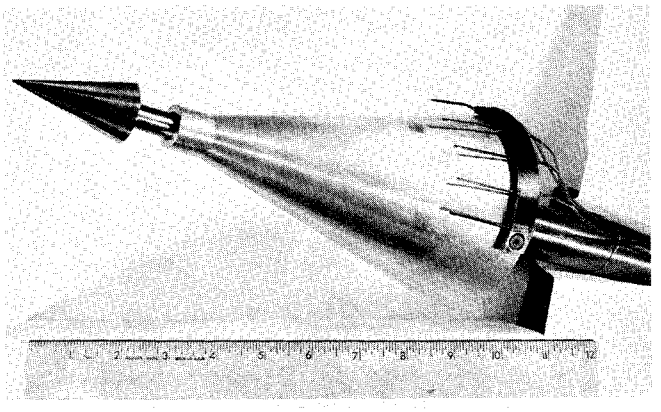

Fig. 6 Aluminum mandrel with stagnation pressure probe assembly mounted.

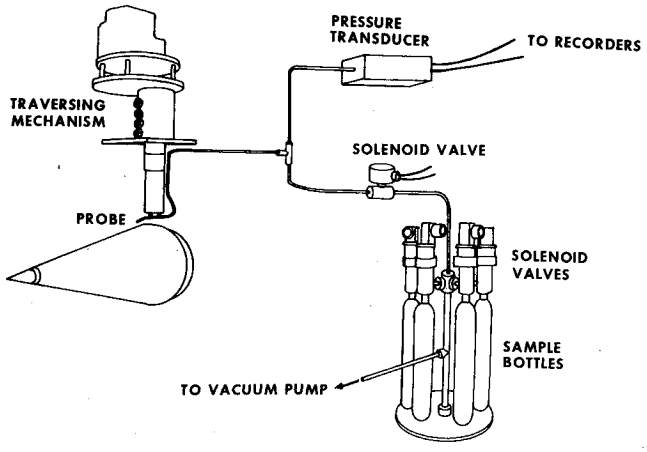

Fig. 7 Gas sampling schematic.

In this manner, the alignment could be checked with a simple set of spacers before casting. The probes were mounted with their centerlines aligned with that of the cone axis to insure that the tips were exposed first. The installation of five such probes on a mandrel is shown in Fig. 6.

Boundary-Layer Profile Instrumentation

Since the receding surface would have placed fixed probes outside the boundary layer after a very short time, a motor-driven traversing mechanism was designed. The position was determined by a 10-turn precision potentiometer. The probes used with the mechanism consisted of a flattened pitot tube, 0.025-in. thick, 0.006-in. opening, and a bare wire (0.021 diam) chromel-alumel thermocouple. The two probes were soldered together to form a y configuration. The linear traversing speed was about 0.08 in./sec.

The probes were mounted so that they could deflect upward when the mechanism contacted the model on the downstroke. This tripped a microswitch located within the probe strut and reversed the direction of travel. At the top of the stroke, the direction was reversed by actuating a relay. The two probes (pressure and temperature) were adjusted to contact the model simultaneously. This reversing method was required to allow a complete traverse of the boundary layer without damaging the probe.

Gas-Sampling Techniques

Determination of ablation product concentration profiles for aromatic hydrocarbons with their attendant pyrolysis or oxidation required a sophisticated sampling probe that would prevent chemical alteration of the sample after it entered the probe. Such a probe was conceptually designed but was not fabricated because of manufacturing technology limitations. Therefore, only carbon-dioxide boundary-layer concentration data were obtained.

As with the other boundary-layer instrumentation, it was found necessary to move the sampling probe as the ablating surfaces receded in order to obtain meaningful samples. For this reason, samples were taken through the traversing boundary-layer pitot probe by installing a solenoid valve that allowed the gas to flow into the collection system, as shown in Fig. 7. These samples were analyzed by means of a mass spectrometer.

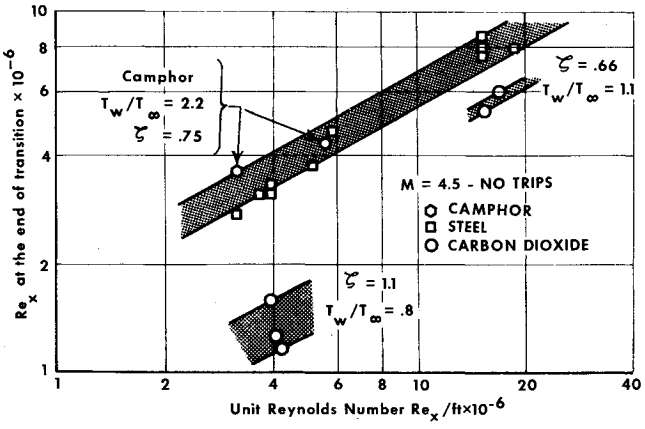

Fig. 8 Boundary-layer transition based on peak heat transfer (steel model) or peak recession rate (ablating model).

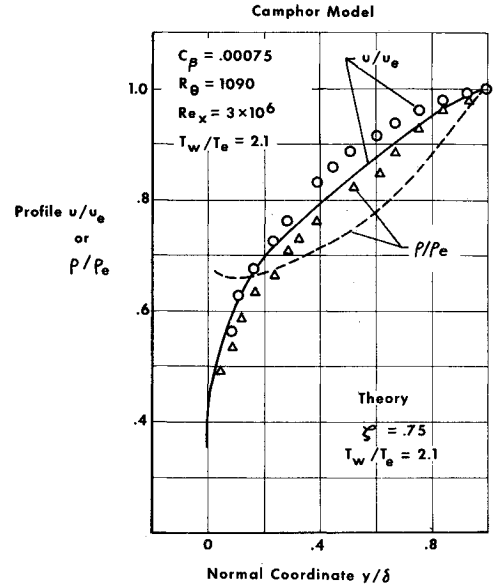

Fig. 9 Comparison of profile data with theory of Ref. 7; camphor model, $Re_x = 3 \times 10^6$.

Results

Since the purpose of this effort was to develop both the techniques and equipment necessary to measure boundary-layer parameters on subliming bodies, not every test produced useful data. However, the information that was obtained is presented in the following sections. Whenever possible, comparisons between the test data and the predictions of Ref. 7

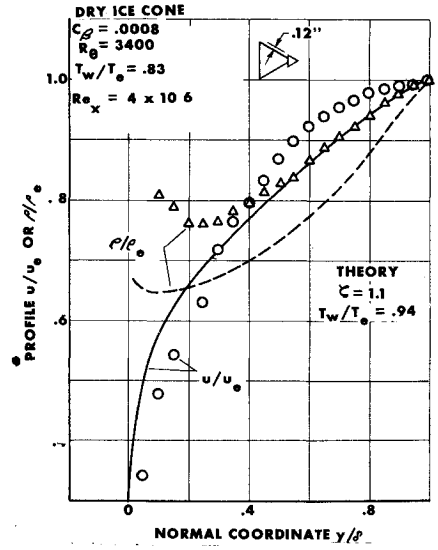

Fig. 10 Comparison of profile data with theory of Ref. 7; dry ice model, $Re_x = 4 \times 10^6$.

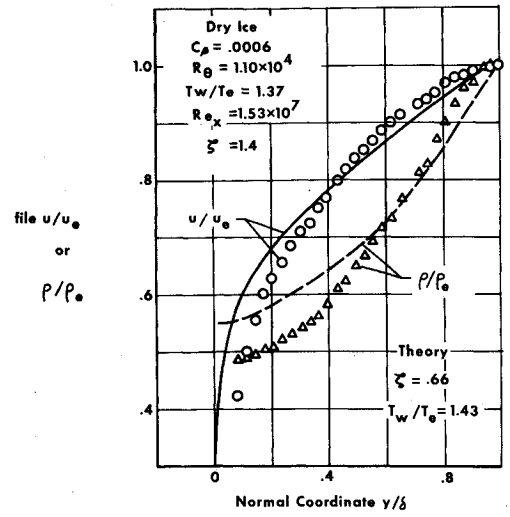

Fig. 11 Comparison of profile data with theory of Ref. 7; dry ice model, $Re_x = 15 \times 10^6$.

are made. In all cases, the models had flush-fitting noses except where noted in the data.

Boundary-Layer Transition

Figure 8 presents a plot of the cone surface Reynolds number corresponding to peak heat transfer or surface recession; a strong effect due to ablation is seen. The usual unit Reynolds number effects are also seen. No trips were used for these data, although the effects of the steel noses used with ablation models cannot be discounted.

Boundary-Layer Velocity and Density Profiles

Typical boundary-layer velocity and density profiles are presented in Figs. 9–11. They were computed from the measured pitot pressure and total temperature survey data and take into account the presence of ablation products.

Similarity between mass and energy diffusion was assumed in order to estimate local gas composition, since inadequate sampling data had been obtained.

Both the velocity and density profiles are compared to the theory of Economos[7] for corresponding values of the blowing parameter as estimated from theory. The velocity profiles are somewhat fuller than theory predicts. The poor agreement of the density profiles with ablation reflects the inability to measure temperatures near the wall.

Skin-Friction Determination

The plotting technique of Clauser was used in conjunction with Economos' theory in an attempt to determine skin

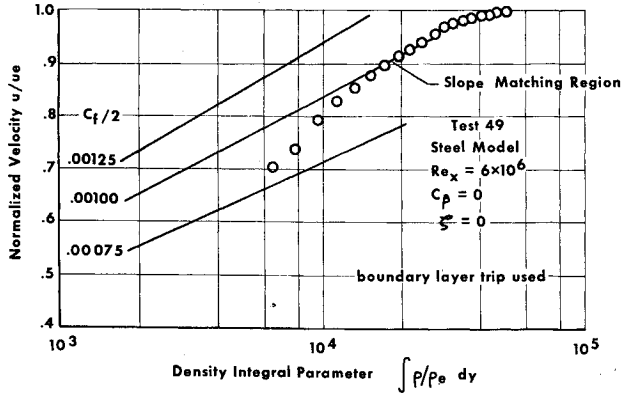

Fig. 12 Clauser skin-friction plot for steel calibration cone.

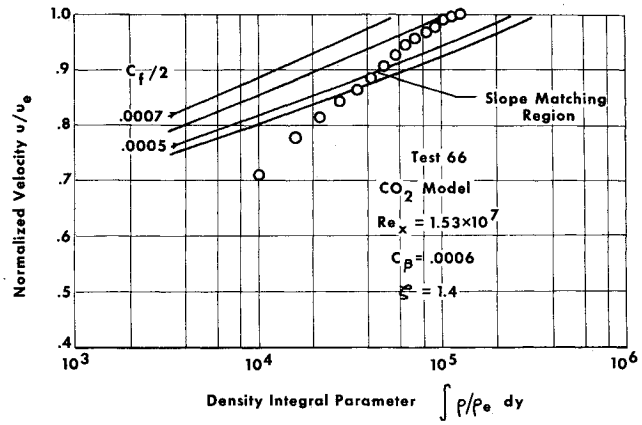

Fig. 13 Clauser skin-friction plot for CO_2 model.

friction from the velocity profiles. Two such plots are given in Figs. 12 and 13. Some of the ice data did not correlate well on this type of plot, probably because it was taken too near to the transition point. Note that test 49 had a boundary-layer trip, and test 66 had a very high unit Reynolds number.

Determination of the proper value of $C_f/2$ from data such as shown in Figs. 12 and 13 requires considerable experience and judgment, since only a very small region of the profile, around $u/u_e = 0.9$, can be expected to match the slope of the theoretical skin-friction lines. In Fig. 15, the proper value of $C_f/2$ is clearly just below 0.001; in Fig. 16, the estimated value was taken as 0.00043, based on similar data from Ref. 7.

Gas-Sample Results

The very limited gas sampling results obtained are given in Fig. 14, as a matter of interest, since insufficient data were obtained for comparison with theory. Test 67, which was a high-unit Reynolds number test, agrees quite well with the theory. Test 61, a low-unit Reynolds number test, gives too low a value of CO_2 concentration, most likely because of an inaccurate measurement.

Recession Measurements

The surface recession data obtained from both the enlarged photographs and the laser surface follower are presented in terms of the nondimensionalized blowing coefficient C_β. The results are given in Figs. 15 and 16 for the CO_2 tests in which the experimental blowing coefficients are compared to Economos' theory for $\zeta = 1.1$ (low Re/ft) and 0.66 (high Re/ft). Figure 17 presents the camphor blowing rate data, again compared to theory. The values of ζ were obtained from an energy balance with specified

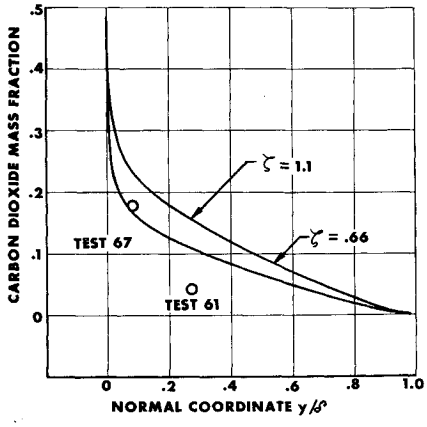

Fig. 14 Boundary-layer sampling results.

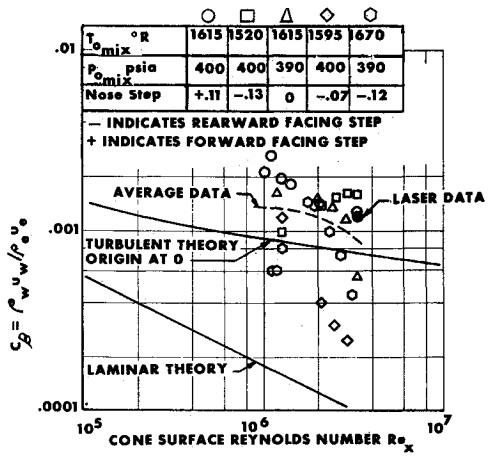

Fig. 15 CO_2 recession data for low-unit Reynolds number tests.

wall temperature (T_{subl}) and assumed unity Prandtl and Lewis numbers. The normalizing edge conditions were obtained by using the Mach number distribution provided by the tunnel calibration data, the tunnel stagnation conditions, and an average total pressure recovery across the cone shock of 0.72.

The photographic recession data exhibit a large amount of scatter from test to test (Fig. 15). The data from any given test form a definite trend, since they are obtained from the displacement of two continuous lines. There is some correlation of C_β with the initial step conditions of the CO_2 models, i.e., high C_β for forward-facing steps and low C_β for rearward-facing steps. An arithmetic average is also shown for the data from the five tests (interpolated points at constant Re_x); it indicates higher C_β's than Economos' theory would predict for $\zeta = 1.1$. This could indicate transition at $Re_x \sim 1 \times 10^6$.

The blowing rate data from the high unit Reynolds number tests (Fig. 16) present an entirely different picture. All of the experimental data lie above the theoretical curve for turbulent flow from the origin, with a peak blowing rate four times the turbulent value. This was attributed to the presence of strong streamwise vortices triggered by the junction between the steel nose and the CO_2 body.

Such vortices may be responsible for the fluting pattern developed on all ablating models at this location. These patterns tended to be self-preserving, with the ablation rates increasing drastically with time in these locations.

The camphor recession data (Fig. 17) are clearly transitional, although again the turbulent peak blowing rates are underestimated.

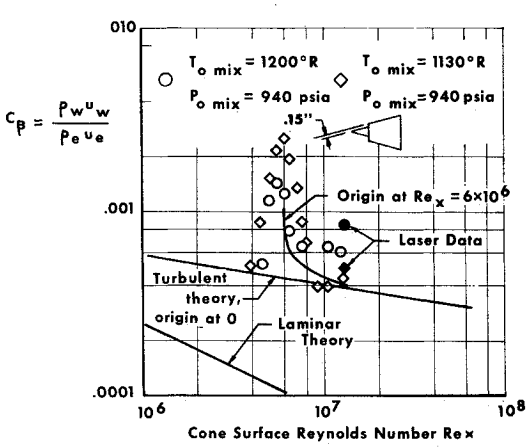

Fig. 16 CO_2 recession data for high-unit Reynolds number tests.

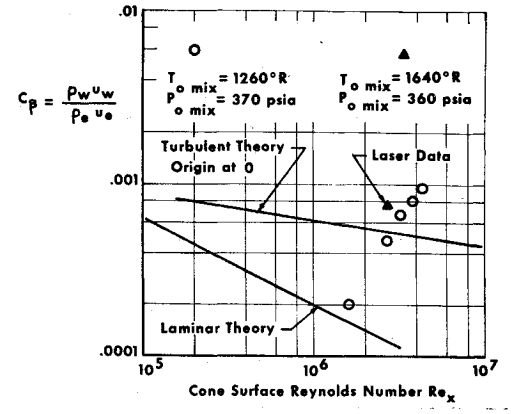

Fig. 17 Camphor model recession data.

The laser recession measurements tend to be somewhat larger. Only the early test-time laser data were used, and sudden ramps in the oscillograph traces clearly indicating model movements were excluded.

Camphor Model Surface Measurements

Static pressure taps

The cone surface pressures were measured on three tests. In each case, the data recorded indicated surface pressure values that were somewhat lower than would be expected for a freestream Mach number of 6.2 and a local cone angle of 15°.

Buried temperature sensors

Although temperature measurements were made on only one test, the technique seemed to work well. The camphor has sufficient insulation value so that submerged thermocouples showed practically no increase in temperature until their exposure. Once the ablative liner receded past their position, the data recorded corresponded very closely to the expected temperature levels.

Submerged stagnation pressure sensors

Two tests were run in which successful measurements were made with buried stagnation pressure probes exposed because of the camphor ablation. It had been anticipated that not only would recession rate data result, but that boundary-layer survey data could also be obtained.

The results of test 59, which employed five submerged probes, are given in Fig. 18. Only three of the five probes indicated a change, and two of these changes occurred near

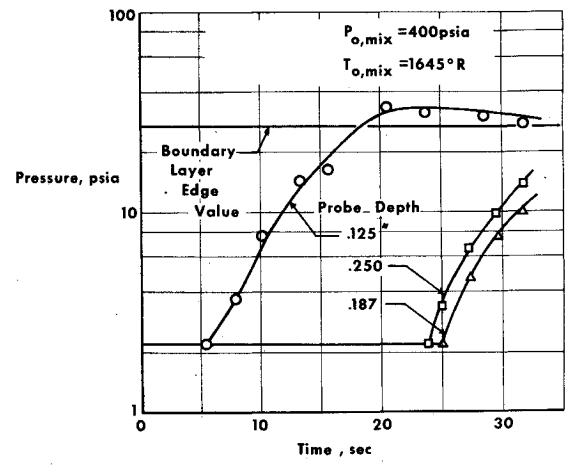

Fig. 18 Submerged Pitot probe data.

Fig. 19 Camphor cone surface detail; $T_{0\,\mathrm{mix}}$ = 1300°R, $P_{0\,\mathrm{mix}}$ = 600 psia.

the end of the test, after significant upstream ablation had occurred, thereby changing the model shape. The ambiguity of the sequence of probes 3 and 4 readings indicated the general deterioration of the surface at this time, manifested as porosity and local severe ablation regions. For this reason, no further use was made of these particular data, which are given in Fig. 18 as an example of the technique only.

Ablated Surface Detail

Both dry-ice and camphor models developed two distinct types of striking and similar surface markings as a result of ablation. First, in the region just downstream of the steel nose, grooves developed along conical rays, more or less evenly spaced along the periphery. Downstream of this first regime, a crosshatched or "waffled" pattern formed. This was particularly visible on the camphor models; somewhat higher blowing rates were required with dry ice to make the pattern discernible. A photograph of typical camphor crosshatching is given in Fig. 19. The average included angle of the diamonds appeared to coincide with twice the Mach angle of the external flow.

Since the grooves in such a pattern represent local regions of intense ablation, this phenomenon could have accounted for some of the recession rate measurements which were well above the theoretical values. A version of the laser surface follower programed to regularly scan some small region of the ablating surface could provide detailed information on the development of these crosshatched patterns.

Conclusions

The primary result of this work is that it has been established that it is possible to make meaningful measurements in boundary layers in the presence of low-temperature sublimation.

Successful model fabrication and instrumentation techniques have been developed; possible further improvements have been identified. The comparison to theory of the limited test results shown is more a vindication of the experimental methods than a test of the validity of the theory.[7] A great deal more data are required for a meaningful test of the theory, which would then allow more rigorous extensions of the test results to re-entry conditions. These preliminary results, however, indicate that the theory tends to underestimate the turbulent blowing rates and that strong local peak ablation regions are present.

References

[1] Adams, M. C., "Recent Advances in Ablation," *ARS Journal*, Vol. 29, No. 9, Sept. 1959, pp. 625–629.

[2] Pettus, J. J., "Persistent Reentry Vehicle Roll Resonance," AIAA Paper 66-49, New York, 1966.

[3] Ericsson, L. E. and Reding, J. P., "Ablation Effects on Vehicle Dynamics," AIAA Paper 66-51, New York, 1966.

[4] Lipfert, F. and Genovese, J., "An Experimental Study of the Boundary Layer on Low Temperature Subliming Ablators," TR-688, Feb. 1968, General Applied Science Labs. Inc., Westbury, N.Y.

[5] Georgiev, S., "Hypersonic Ablation and Interpretation of Test Results," RR 99-1960, Avco-Everett Research Labs., Wilmington, Mass.

[6] Libby, P. A., "Similarity Parameters for Subliming Bodies in Hypersonic Flow," TR-453, Sept. 1964, General Applied Science Labs. Inc., Westbury, N.Y.

[7] Economos, C., "Compressible Turbulent Boundary Layer with Mass Transfer," Doctoral dissertation, Polytechnic Institute of Brooklyn, Dept. of Aeronautics and Astronautics, Farmingdale, N.Y.; also AIAA Preprint 69-161.

[8] Weiss, R., "Sublimation of a Hemisphere in Supersonic Flow," AFOSR-TN-59-870, July 1959, Air Force Office of Scientific Research, Washington, D.C.